Tribol Lett (2007) 28:9–17
DOI 10.1007/s11249-007-9242-9

ORIGINAL PAPER

A Model for Magnetic Tape/Guide Friction Reduction by Laser Surface Texturing

Bart Raeymaekers · Izhak Etsion · Frank E. Talke

Received: 14 March 2007 / Accepted: 11 June 2007 / Published online: 6 July 2007

Abstract The friction coefficient between a magnetic tape and a guide in a tape path can be minimized by creating micro dimples on the guide surface with laser surface texturing. The dimples enhance the formation of an air bearing and reduce the friction coefficient between the tape and the guide due to the increased spacing. A model is presented to optimize the geometry of the surface texturing parameters to maximize the average air bearing pressure and minimize the tape/guide friction coefficient.

Keywords Magnetic tape tribology · Friction modeling · Surface texturing

Nomenclature

c	Minimum tape/guide spacing
$H(X,Y)$	Dimensionless spacing, $H = h/c$
$H^*(X^*,Y^*)$	Dimensionless spacing in local coordinates, $H^* = h^*/c$
$h(x,y)$	Tape/guide spacing in global coordinates
$h^*(x^*,y^*)$	Tape/guide spacing in local coordinates
h_p	Depth of dimple
N	Number of dimples in a column
$P(X,Y)$	Dimensionless pressure, $P = p/p_a$
$p(x,y)$	Air bearing pressure
p_a	Atmospheric pressure
p_{avg}	Average air bearing pressure
r_1	Imaginary cell half length
r_p	Dimple radius
R	Guide radius
S_p	Dimple area density
T	Tape tension per unit tape width
w	Width of the tape
X, Y	Dimensionless coordinate, $X = x/r_p$, $Y = y/r_p$
X^*, Y^*	Dimensionless local coordinate, $X^* = x^*/r_p$, $Y^* = y^*/r_p$
x, y	Global coordinate
x^*, y^*	Local coordinate
δ	Dimensionless minimum tape/guide spacing, $\delta = c/2r_p$
ε	Dimple aspect ratio, $\varepsilon = h_p/2r_p$
γ	Over-relaxation parameter
λ	Flow parameter, $\lambda = 3\mu_a U/2r_p p_a$
σ_s	Standard deviation of asperity summit heights

B. Raeymaekers (✉) · F. E. Talke
Center for Magnetic Recording Research, University of California San Diego, La Jolla, CA 92093, USA
e-mail: bart@talkelab.ucsd.edu

I. Etsion
Department of Mechanical Engineering, Technion, Haifa 32000, Israel

Introduction

Lateral tape motion (LTM) is defined as the time-dependent motion of magnetic tape perpendicular to the tape transport direction, and is one of the critical parameters in the design of magnetic tape drives. LTM is a friction related problem that can cause track misregistration and that limits the achievable track density on a tape [1]. LTM is influenced by friction between tape and guide surfaces and by the dynamics of the tape and the guides. It was shown in [2–4] that friction attenuates LTM. On the other hand, tape drives with low-friction pressurized air bearing guides yield a significantly lower LTM than tape drives with rotating guides [5]. The main disadvantage of pressurized air bearing guides is that they

require an external compressor which is undesirable from a reliability point of view.

To achieve low friction between a tape and a guide without external pressurization, the use of a self acting air bearing between the tape and guide is desirable. This would eliminate the need for an external compressor, while still benefiting from the low friction of an air bearing. In studying the friction of the tape/guide interface, it was observed [6] that the tape speed at which the transition from boundary lubrication to hydrodynamic lubrication occurs, is strongly influenced by the surface roughness of the guides. In [7] laser surface textured guides were used and it was found that laser texturing reduces the friction coefficient between tape and guide significantly, especially in the low tape speed range. In this article, we study the effect of laser surface texturing (LST) on the tribological performance of the magnetic tape/guide interface and the transition from boundary lubrication to hydrodynamic lubrication with the intent to reduce friction and minimize the tape speed at which the transition occurs.

Laser surface texturing is a well established technique to create micro dimples on the surface of tribological components [8–11]. These dimples are generally arranged in columns and act as micro-hydrodynamic bearings, i.e., they create a local pressure increase between two surfaces in relative motion. Hence, the fluid film thickness for such bearings is increased. Figure 1 shows a tape moving at a speed U over a laser surface textured guide. The size of the dimples is exaggerated for the purpose of clarity.

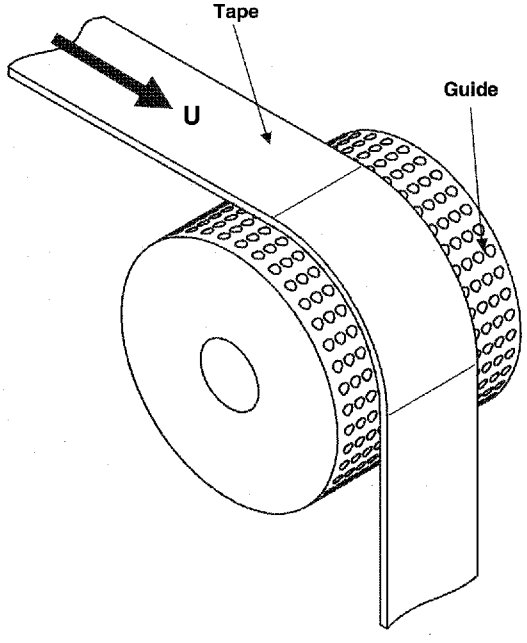

Fig. 1 Tape moving over a laser surface textured guide

Theoretical Model

To better understand the effect of a textured guide surface on the tribological performance of the tape/guide interface, we have simulated the pressure distribution between the tape and the guide surface for a column of ten dimples. We made the following assumptions:

1. The tape is considered rigid. Local elastic deformations of the tape are neglected. This assumption implies that no elasto-hydrodynamic effects are taken into account.
2. The tape is assumed to be conformal to the guide [12]. This case is identical to a parallel slider bearing. One-dimensional foil bearing simulations [13] show that the tape is indeed conformal to a smooth guide over 95% of the interface length.
3. The shape of all dimples is identical and spherical. The dimples are uniformly distributed over the guide surface.
4. The gas in the air bearing is compressible and has a constant viscosity.
5. The air bearing is assumed to be infinitely wide, i.e., side flow effects are neglected. Hence, one column of dimples is representative of the whole air bearing surface, when a periodic boundary condition is applied in the direction perpendicular to the flow.
6. The model is only valid for the hydrodynamic lubrication regime. No asperity contact is allowed.

According to assumption 1, the guide and magnetic tape are separated by a uniform air film of thickness c. It should be noted that in reality the tape is flexible, i.e., simultaneous solution of the Reynolds equation along with the tape elasticity equation is required. However, the assumption of a rigid tape allows a first order approximation of the physical situation without the need for extended numerical solutions.

The effects of the curvature of the cylindrical surface can be neglected in the model, since the minimum tape/guide spacing c is much smaller than the guide radius. Additionally, we assume full fluid film lubrication and therefore require $c \geq 3\sigma_s$ [14].

The spherical dimples are uniformly distributed over the guide surface and each dimple is contained within an imaginary square cell of length $2r_1$. Figure 2 shows one dimple with radius r_p, positioned at the center of the imaginary cell. We have defined a local Cartesian coordinate system x^*y^* with origin at the center of the imaginary cell.

The cell length r_1 can be expressed as a function of the dimple area density S_p, and the dimple radius r_p, as

$$r_1 = \frac{r_p}{2}\sqrt{\frac{\pi}{S_p}} \tag{1}$$

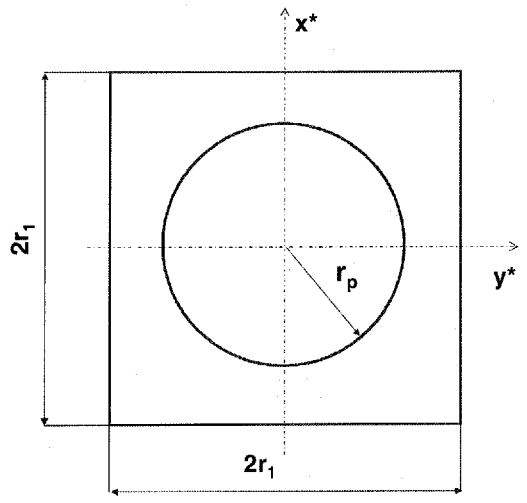

Fig. 2 Single spherical dimple within its imaginary cell (local coordinates)

Figure 3a shows the distribution of the dimples on the guide surface in a global Cartesian *xy* coordinate system. Each column of dimples is parallel to the *x*-axis and can be modeled as shown in Fig. 3b.

Figure 4 presents a cross section through the center of the dimples. Here, r_p denotes the radius of the dimple, h_p denotes the depth of the dimple, c is the tape/guide minimum spacing and $h(x,y)$ is the clearance between the guide surface and the magnetic tape.

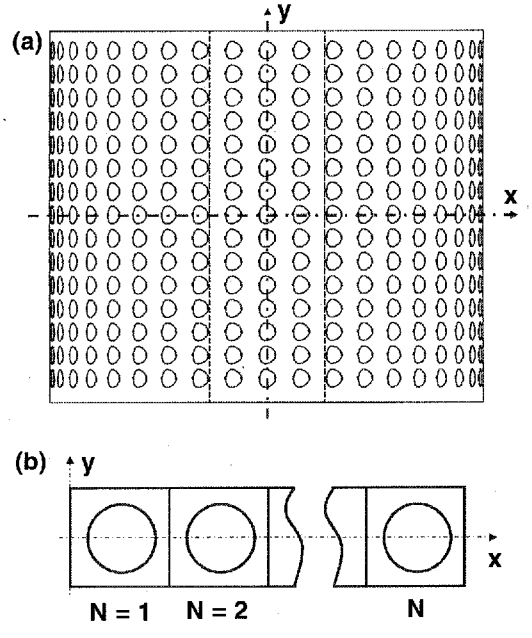

Fig. 3 (**a**) Dimple distribution and (**b**) a single column of dimples (global coordinates)

The two dimensional, steady-state compressible Reynolds equation, which relates the pressure distribution to the spacing at the tape/guide interface [15], is given by

$$\frac{\partial}{\partial x}\left(ph^3\frac{\partial p}{\partial x}\right)+\frac{\partial}{\partial y}\left(ph^3\frac{\partial p}{\partial y}\right)=6\mu_a U\frac{\partial(ph)}{\partial x} \tag{2}$$

where x and y represent coordinates in a global Cartesian coordinate system, $p(x,y)$ is the air bearing pressure, μ_a is the dynamic viscosity of air and $h(x,y)$ is the local clearance between tape and guide. Since the tape/guide spacing is much larger than the mean free path of air, rarefaction effects are neglected.

For the analysis of the textured surface, it is convenient to introduce the following non-dimensional expressions:

$$X=\frac{x}{r_p},\quad Y=\frac{y}{r_p},\quad P(X,Y)=\frac{p(x,y)}{p_a},\quad H(X,Y)=\frac{h(x,y)}{c}, \tag{3}$$

where X and Y denote the non-dimensional (global) coordinates, and P and H denote the non-dimensional pressure and spacing, respectively. The normalizing pressure p_a is the atmospheric pressure. The dimensionless local spacing H^* as a function of the dimensionless local coordinates X^*,Y^* for one cell, shown in Fig. 4, is given by [16]:

$$\begin{aligned} H^*(X^*,Y^*)&=1,\quad \text{for } X^{*2}+Y^{*2}>1\\ H^*(X^*,Y^*)&=1+\sqrt{\left(\frac{\varepsilon}{2\delta}+\frac{1}{8\varepsilon\delta}\right)^2-(X^{*2}+Y^{*2})\frac{1}{4\delta^2}}\\ &\quad-\left(\frac{1}{8\varepsilon\delta}-\frac{\varepsilon}{2\delta}\right),\quad \text{for } X^{*2}+Y^{*2}\le 1 \end{aligned} \tag{4}$$

where $\varepsilon = h_p/2r_p$ is the aspect ratio of the dimple and $\delta = c/2r_p$ is the dimensionless tape/guide minimum spacing.

To create a column of dimples of identical shape (see Fig. 3b), we expand the dimensionless height distribution for a single cell, $H^*(X^*,Y^*)$, to a column of $N = 10$ cells by repeating the height distribution for a single cell for each cell in the column. The dimensionless Reynolds equation in the global coordinate system can then be expressed as

$$\frac{\partial}{\partial X}\left(PH^3\frac{\partial P}{\partial X}\right)+\frac{\partial}{\partial Y}\left(PH^3\frac{\partial P}{\partial Y}\right)=\frac{\lambda}{\delta^2}\frac{\partial(PH)}{\partial X} \tag{5}$$

where $\lambda = 3\mu_a U/2r_p p_a$ and $\delta = c/2r_p$.

The following boundary conditions are assumed. The pressure is atmospheric at the inlet and outlet of the tape/guide interface. In addition, the pressure is periodic in the direction perpendicular to the air flow (Y-direction). This

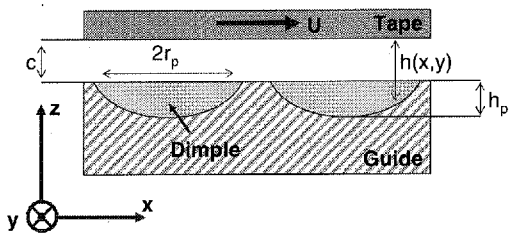

Fig. 4 Geometry of the dimples

assumption implies that side-flow effects are neglected. Multiple columns of dimples next to one another will yield a periodic pressure distribution. The period is defined by the size of the imaginary cell ($2r_1$). The boundary conditions can be expressed as

$$\begin{gathered} P(X=0,Y)=1 \\ P\left(X=N\tfrac{2r_1}{r_p},Y\right)=1 \\ \tfrac{\partial P}{\partial Y}\left(X,Y=-\tfrac{r_1}{r_p}\right)=\tfrac{\partial P}{\partial Y}\left(X,Y=\tfrac{r_1}{r_p}\right)=0 \end{gathered} \tag{6}$$

where N is the number of cells in a column (see Fig. 3b). Equation (5) can be solved for the pressure distribution if the dimensionless spacing $H(X,Y)$ and the dimensionless parameters λ, δ and ε are specified. A "staggered grid" finite difference approach [17] was used to solve Eq. (5) with the boundary conditions specified in Eq. (6) for a non-dimensional local spacing distribution given by Eq. (4). A grid of 200 by 200 nodes per cell was chosen based on convergence requirements. Due to the symmetry with respect to the X-axis, it is only necessary to solve for half the imaginary cell. An over-relaxation factor of $\gamma = 1.4$ was used to obtain a faster convergence of the pressure distribution.

Results

Air Bearing Pressure

Figure 5a depicts the cross section of the column of dimples along the X-axis (see Fig. 3b), normalized by r_p. The horizontal and vertical scales in Fig. 5a are uneven, resulting in the distorted appearance of the dimple shape. Figure 5b shows the dimensionless pressure distribution along the X-axis, for a column of $N = 10$ cells and values of $\lambda = 2.14E{-}5$, $\delta = 0.002$, $\varepsilon = 0.01$ and $S_p = 0.15$. Figure 5c shows the two dimensional pressure distribution across a single dimple in a column (imaginary cell).

The direction of the flow (tape speed U) has been indicated in Fig. 5. From Fig. 5b we observe that the pressure at the inlet of a dimple (with reference to the direction of the flow) becomes sub-ambient, because the

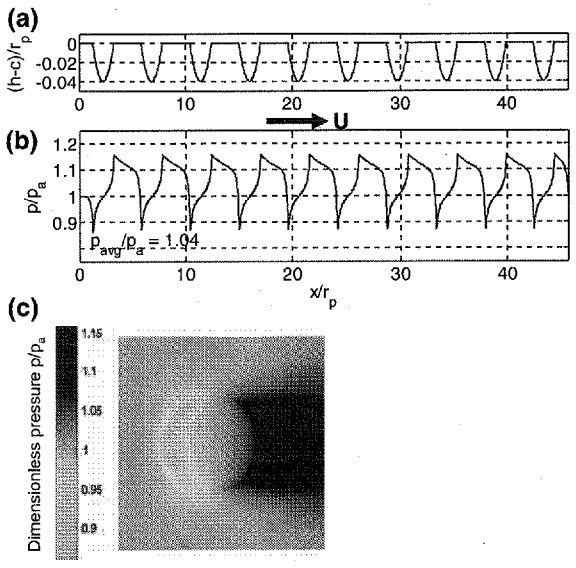

Fig. 5 (**a**) Cross-sectional view of the column of dimples, (**b**) Dimensionless pressure distribution along the X-axis for a column of $N = 10$ dimples and (**c**) pressure distribution across a single dimple (imaginary cell). Dimple density $S_p = 0.15$

local spacing between the tape and guide increases. When the flow passes the midpoint of the dimple, the spacing decreases and thus, the pressure increases. The pressure distribution is non-symmetric over the dimple region, i.e., the net effect of the dimples is an increased average air bearing pressure p_{avg}, which is greater than the atmospheric pressure p_a, i.e., $p_{avg}/p_p > 1$. Without dimples, the dimensionless pressure $p_{avg}/p_a = 1$, equivalent to the parallel slider case. The increased pressure p_{avg} will increase the load bearing capacity and spacing between the tape and the guide for a fixed tape tension and speed. In other words, for a dimpled guide surface, the transition from boundary lubrication to hydrodynamic lubrication occurs at a lower tape speed than in the case of a smooth guide. We point out that a single column of five to ten consecutive dimples is representative of the entire dimpled surface. As observed in Fig. 5, the pressure profile becomes identical for each dimple, except for the first two dimples at the inlet and outlet of the column. Therefore, the simulation of just one column of ten dimples is a valid representation for the effects of a complete textured surface.

Optimization of Dimple Geometry

The dimensionless parameters S_p, ε, δ, and λ define the dimple area density, dimple aspect ratio, the dimensionless minimum spacing between tape and guide and the flow parameter, respectively. Table 1 shows a typical reference case along with the range of variation of the dimple depth and tape/guide spacing as well as the corresponding

Table 1 Range of the dimensional and dimensionless parameters

Parameter	Minimum	Reference	Maximum
h_p (μm)	0.3	1	5
c (nm)	100	200	400
ε	0.003	0.01	0.05
δ	0.001	0.002	0.004
λ	5E-06	2E-05	3E-05

dimensionless parameters. The atmospheric pressure p_a was taken to be 0.1 MPa and the viscosity of air - $\mu_a = 1.81E{-}5$ Pas. The typical standard deviation of asperity summit heights in commercial tape/guide contacts is on the order of $\sigma_s = 30$ nm [7]. This number is the equivalent roughness of the mating tape and guide surfaces, see McCool [18]. The assumption of full fluid film lubrication, $c \geq 3\sigma_s$ [14], requires the minimum tape/guide spacing c to be larger than 100 nm. The dimple radius was selected to be $r_p = 50$ μm for ease of manufacturing.

In the following, we use our model to numerically investigate how these parameters can be chosen to yield the highest possible average air bearing pressure between the conformal tape and the guide. A maximized average air bearing pressure will yield the highest load carrying capacity and hence, the highest tape/guide spacing for a given tape tension.

Figure 6 shows the dimensionless average air bearing pressure p_{avg}/p_a versus the dimple density S_p for different values of the dimple aspect ratio ε and for the reference values $\delta = 0.002$ and $\lambda = 2E\text{-}5$.

Since the guide surface is smooth (parallel slider bearing) for both of the extreme dimple densities $S_p = 0$ and $S_p = 1$, an optimum density must exist which yields the highest average air bearing pressure p_{avg}/p_a. From Fig. 6 we observe that the optimum S_p occurs for values from 0.10 to 0.30 depending on the dimple aspect ratio ε. We note that the optimum dimple density shifts towards lower values for an increasing dimple aspect ratio ε. Hence, when the dimple aspect ratio is increased, fewer dimples per unit surface area are needed to obtain the maximum dimensionless air bearing pressure for that specific dimple aspect ratio. We also found that the dimensionless tape/guide minimum spacing δ does not affect the optimum dimple density. Additionally, it is clear from Fig. 6 that an optimum dimple aspect ratio exists in the range $0.003 \leq \varepsilon \leq 0.05$.

Figure 7a shows the dimensionless pressure versus the dimple aspect ratio for different values of the dimensionless spacing δ and for $\lambda = 2 \times 10^{-5}$ and a dimple density $S_p = 0.15$. Figure 7b shows the dimensionless pressure versus the dimple aspect ratio for different values of the parameter λ and for $\delta = 0.002$. For a given ε and for a constant atmospheric pressure p_a, dimple radius r_p and air viscosity μ_a, the flow parameter λ depends only on the tape speed U.

From both Fig. 7a and b we observe that the optimum value for the dimple aspect ratio ε is approximately 0.006 regardless of δ or λ. For instance, if the dimple radius $r_p = 50$ μm, we observe that the optimal value of the dimple depth $h_p = 0.6$ μm. From Fig. 7a and b we also note that the dimensionless average air bearing pressure

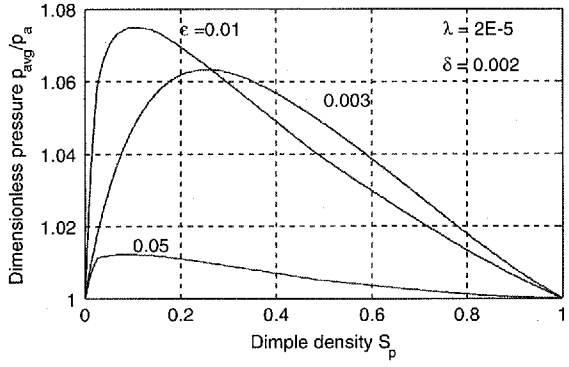

Fig. 6 Dimensionless average air bearing pressure, p_{avg}/p_a versus dimple density S_p

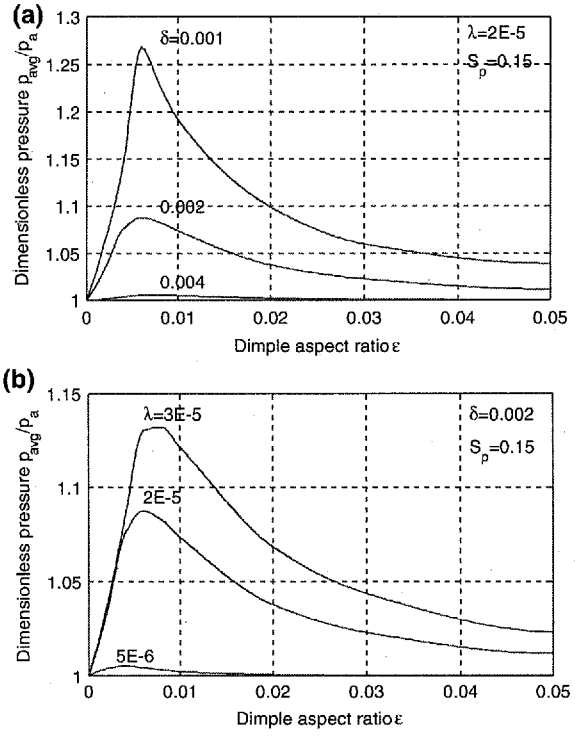

Fig. 7 Dimensionless average air bearing pressure versus dimple aspect ratio for (**a**) different dimensionless spacing values and (**b**) different values of λ

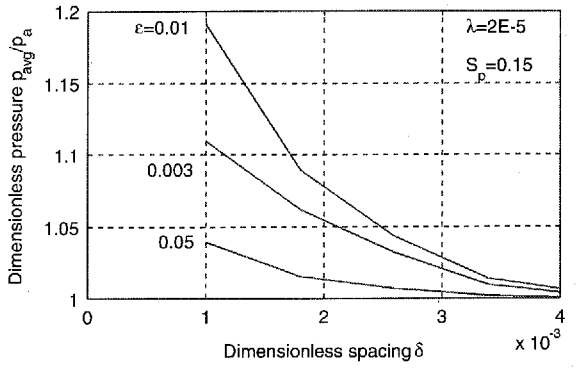

Fig. 8 Dimensionless average air bearing pressure versus dimensionless spacing for different dimple aspect ratios

increases for decreasing δ and for increasing tape speed U (increasing λ), as would be expected.

Figure 8 shows the dimensionless average pressure p_{avg}/p_a versus the dimensionless spacing $\delta = c/2r_p$ for different values of the dimple aspect ratio ε and for $S_p = 0.15$ and λ = 2E-5.

The results are shown for $\delta \geq 0.001$ only, corresponding to full fluid lubrication. We observe a sharp increase in the dimensionless pressure for decreasing values of δ, which corresponds to decreasing tape/guide spacing.

Finally, Fig. 9 shows the optimum combination of dimple density and dimple aspect ratio, for different values of the dimensionless tape/guide minimum spacing and for λ = 2E-5.

We observe that for the optimum dimple aspect ratio $\varepsilon = 0.006$ and the optimum dimple density $S_p = 0.15$, the dimensionless pressure reaches a maximum value of approximately 1.09 for $\delta = 0.002$ and λ = 2E-5. This number represents the maximum dimensionless average pressure that can be obtained, according to our simplified model.

Friction

When neglecting the tape bending stiffness, the equilibrium between the tape tension per unit tape width, T, and the air bearing pressure requires that [19]

$$p_{avg} - p_a = T/R, \tag{7}$$

for a guide with radius R. Non-dimensionalizing Eq. (7) with the atmospheric pressure p_a yields

$$p_{avg}/p_a - 1 = T/(p_a R) \tag{8}$$

Figure 10 shows the dimensionless tape/guide spacing δ versus the dimple aspect ratio ε for different values of the dimensionless tape tension $T/(p_a\ R)$ (dimple density S_p = 0.15 and flow parameter λ = 2E-5). The results shown in Fig. 10 were obtained from $p_{avg}/p_a = f(\delta)$ curves as shown in Fig. 8. The intersection of these curves with horizontal lines for p_{avg}/p_a = constant yields values of δ for each ε-curve. The dimensionless average air bearing pressure was then converted to a dimensionless tape tension by eq. (8). To obtain Fig. 10, we considered more values of than displayed in Fig. 8.

Since we assumed that the tape and guide are conformal, Fig. 10 shows the dimensionless tape/guide spacing which is only due to the pressure generated by the presence of dimples in the tape/guide interface. The results presented in Fig. 10 were obtained for $\delta > 0.001$ to comply with the assumption of full fluid film lubrication. We observe that the optimum dimple aspect ratio $\varepsilon = 0.006$ maximizes the tape/guide spacing regardless of the tape tension, since this optimum aspect ratio always yields the highest average pressure. For any given ε value, the dimensionless tape/guide spacing decreases when the dimensionless tape tension is increased, as would be expected. We observe that

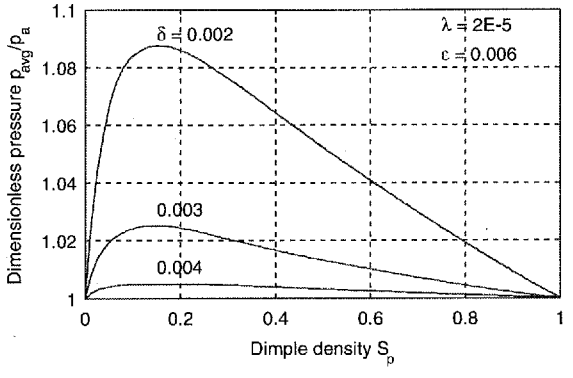

Fig. 9 Dimensionless average air bearing pressure versus dimple density S_p, for the optimum dimple aspect ratio

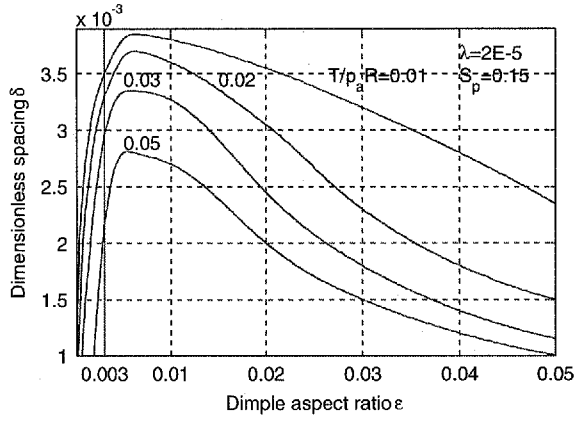

Fig. 10 Dimensionless tape/guide spacing δ versus the dimple aspect ratio ε for different values of the dimensionless tape tension

the dimensionless spacing δ is very sensitive to the dimple aspect ratio when $\varepsilon < 0.006$. This is further amplified when the dimensionless tape tension is increased.

The average shear stress in the air bearing, which is a measure of the air friction, can be expressed as

$$\tau = \mu_a U / c_{eq} \tag{9}$$

where τ is the shear stress, μ_a is the air viscosity and U is the tape speed. The spacing c_{eq} is an equivalent tape/guide spacing that takes into account the dimple depth [15] and can be determined as

$$c_{eq} = c + h_{eq} \tag{10}$$

In Eq. (10), h_{eq} can be obtained by dividing the volume of a dimple by the surface area of its imaginary square cell. Hence,

$$h_{eq} = \frac{h_p S_p}{6 r_p^2}\left(h_p^2 + 3 r_p^2\right) \tag{11}$$

Non-dimensionalizing Eq. (11) with $2r_p$ yields

$$\delta_{eq} = \delta + \frac{2}{3}\varepsilon S_p\left(\varepsilon^2 + \frac{3}{4}\right) \tag{12}$$

which, for $\varepsilon \leq 0.05$, can be approximated by

$$\delta_{eq} = \delta + \varepsilon S_p / 2 \tag{13}$$

If $\tau = f(\delta)$ and $\delta = f(\varepsilon)$ are known (see Eqs. (9)–(13) and Fig. 10), one can determine the relationship between the shear stress τ and the dimple aspect ratio ε. Equation (9) can be re-written in terms of δ_{eq} as

$$\tau = \frac{\mu_a U}{2 r_p \delta_{eq}} \tag{14}$$

The dimensionless shear stress, or equivalently, the friction coefficient, can be obtained as

$$\frac{\tau}{p_{avg} - p_a} = \frac{\mu_a U}{2 r_p \delta_{eq}\left(p_{avg} - p_a\right)} \tag{15}$$

Using the non-dimensional flow parameter $\lambda = 3\mu_a U/2r_p p_a$ and substituting Eq. (7) in Eq. (15), we obtain:

$$\frac{\tau}{p_{avg} - p_a} = \frac{\lambda}{3\delta_{eq}}\frac{p_a R}{T} \tag{16}$$

Equation (16) represents the friction coefficient $\tau/(p_{avg}-p_a)$ of the air bearing, generated by presence of the dimples. Figure 11 shows the friction coefficient $\tau/(p_{avg}-p_a)$ versus the dimple aspect ratio ε for different values of the dimensionless tape tension with a dimple density $S_p = 0.15$ and a flow parameter $\lambda = 2E\text{-}5$.

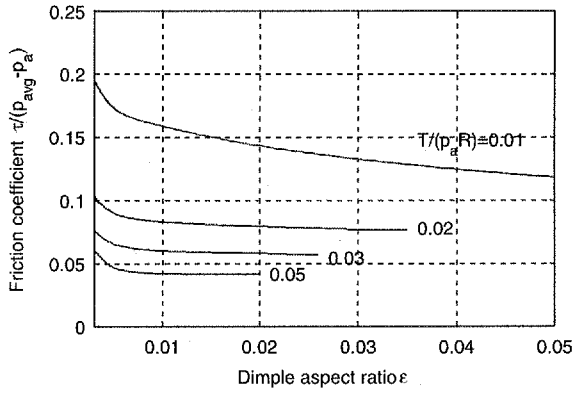

Fig. 11 Dimensionless shear stress versus the dimple aspect ratio ε for different dimensionless values of the tape tension

From Fig. 11 we observe that for a dimensionless tape tension below 0.02, the dimensionless shear stress decreases monotonically as the dimple aspect ratio increases. For a dimensionless tape tension above 0.02 the dimensionless shear stress initially decreases with increasing dimple aspect ratio, but then levels off for aspect ratios above 0.01. This behavior can be understood from the results in Fig. 10 and from Eqs. (13) and (16). As can be seen from Fig. 10 for $\varepsilon < 0.006$, a small increase in ε results in a large increase in δ and hence, from Eqs. (13) and (16), a large increase in δ_{eq} and a large decrease in the friction coefficient, respectively. On the other hand at $\varepsilon > 0.01$ (see Fig. 10) an increase in ε may be compensated by a decrease in δ when calculating δ_{eq}, thereby leaving the friction coefficient unchanged. This is not the case for a low tape tension where an increase in ε above 0.01 results in a relatively small decrease in δ (see Fig. 10) causing δ_{eq} to increase and the friction coefficient to decrease. As a result, the optimum dimple aspect ratio $\varepsilon = 0.006$ which yields maximum load bearing capacity does not provide a minimum for the friction coefficient.

Finally, we observe from Fig. 11 that the friction coefficient decreases for increasing non-dimensional tape tension $T/(p_a R)$, regardless of the dimple aspect ratio ε in accordance with Eq. (16).

Numerical Example

In this section we have compared the predictions of our simplified numerical model with experimental results. We have used the experimental set-up and procedure outlined in [6] and [7] to measure the friction coefficient between a tape and a guide at tape speeds between 4 and 7 m/s, to make sure the tape operates under full fluid lubrication

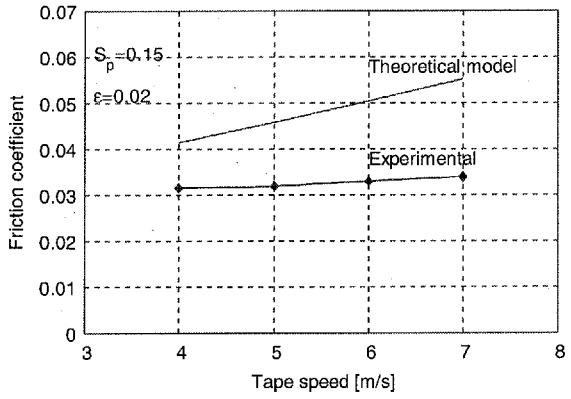

Fig. 12 Friction coefficient versus tape speed for an LST guide of radius 15 mm, $S_p = 0.15$ and $\varepsilon = 0.02$

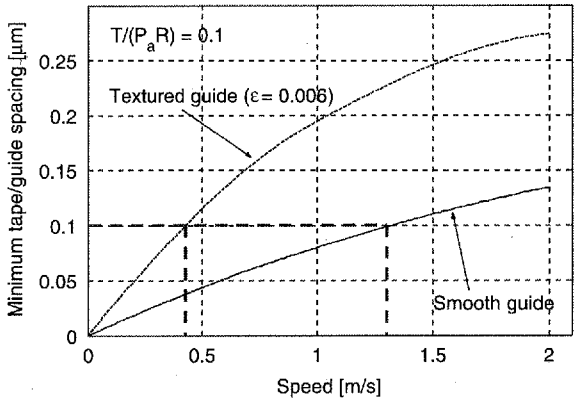

Fig. 13 Minimum spacing c versus tape speed for a dimensionless tape tension of $T/(p_a R) = 0.1$

conditions. Figure 12 shows a comparison between the theoretical predictions and experimental results for a textured guide with a radius R of 15 mm, dimple density $S_p = 0.15$, and dimple aspect ratio $\varepsilon = 0.02$. The tape was a commercial MP tape of width $w = 0.0127$ m. The tape tension was 1 N and the atmospheric pressure $p_a = 0.1$ MPa, i.e., $T/(p_a R) = 0.05$.

The theoretical model is in good agreement with experimental measurements. In the full fluid lubrication regime, the friction coefficient increases slightly for increasing tape speed as predicted qualitatively by the Stribeck curve. The experimental results show that the friction coefficients predicted by the model are of the same order as the experimental results. We note that the values for the theoretical results are higher than those for the experimental results. This is likely due to the simplifying assumption of a conformal and "rigid" tape. A converging channel at the leading edge would create a higher average pressure and thus a higher load bearing capacity. This would result in lower friction coefficients, which would improve the agreement between the theoretical model and experimentally obtained friction coefficients.

Transition Speed Estimation

In the design of tape drives, it is important to minimize the speed at which the transition from boundary lubrication to hydrodynamic lubrication occurs. For a typical smooth guide with $\sigma_s = 30$ nm, hydrodynamic lubrication occurs for a tape/guide spacing of approximately $c = 100$ nm [14]. Figure 13 shows the minimum tape/guide spacing c versus the tape speed for a dimensionless tape tension $T/(p_a R) = 0.1$, for a smooth and a textured guide.

The results in Fig. 13 were obtained by superimposing the spacing due to the presence of dimples in the tape/guide interface, calculated with our model, on the spacing calculated for a smooth guide with [13]. This approach neglects non-linear effects of the compressible air bearing. However, since compressibility effects are small at low velocity, it can be justified that the total tape guide/spacing for a dimpled guide is, to a first order, the sum of the spacing of a smooth guide and the extra spacing created by the presence of dimples in the tape/guide interface.

In Fig. 13, a horizontal line for $c = 3\sigma_s$ yields the transition speed between boundary and hydrodynamic lubrication for both the smooth and the textured guide [14]. For a $3\sigma_s$-value of 100 nm, we observe from Fig. 13 that in the case of a textured guide (dashed line) the transition speed is 0.4 m/s, while in the case of a smooth guide the transition speed is 1.35 m/s. Similarly, for a $3\sigma_s$-value of 130 nm, the transition speed for a textured guide would be 0.55 and 2 m/s in the case of a smooth guide.

Discussion

Our model predicts that dimpled guides feature a significantly lower transition speed between boundary lubrication and hydrodynamic lubrication than smooth guides. Using dimpled guides (stationary) in commercial tape drives instead of the currently used smooth rollers (rotating), would potentially yield improvements in terms of tape transport and LTM. Furthermore, tape wear, which is a problem of considerable interest in tape drives with smooth stationary guides, will also be reduced due to the lower transition speed.

Additionally, dimpled guides would potentially enable the wide-spread introduction of metal evaporated (ME) tape. ME tape is desirable from a magnetics point of view, since the cobalt magnetic layer has a higher coercivity than the currently used metal particulate (MP) tape. Hence, ME tape would allow an increase in storage density, compared to MP tape. The tribological performance of ME tape, however, is problematic compared to MP tape, especially

at low-tape speeds, where surface contact occurs between the tape and the guide surface [6, 20, 21]. Dimpled guide surfaces create a higher air bearing pressure compared to smooth guides and thus, increase the flying height at low speeds. This would improve the tribological performance of ME tape.

Our model neglects elasto-hydrodynamic effects. However, for low tape speeds corresponding to the transition from boundary to hydrodynamic lubrication, the bearing number is small and thus the compressibility effects of the air bearing are less prominent, i.e., it is justifiable to approximate the compressible air bearing by an incompressible one.

Including elasto-hydrodynamic effects in the model would yield a more accurate solution than our current model, but would require a substantially larger numerical effort. For a full-size simulation of the complete tape/dimpled guide interface we calculate the following scenario. Assuming a guide with a radius of 10 mm, a dimple density of 0.2 and a dimple radius of 50 μm, in combination with a 12.7 mm wide tape and a wrap angle of 90 degrees, we calculate that the tape/guide interface contains approximately 20,000 dimples. To fully capture the pressure gradient created over a dimple, a grid of 200 by 200 nodes per dimple (imaginary cell) is needed. Hence, 800 million nodes would be required to simulate the complete tape/guide interface. A numerical problem of this size poses a challenge to present day computer hardware and requires long simulation times, if at all it is solvable.

Conclusion

- The optimum dimple density was found to be between 0.1 and 0.3, depending on the dimple aspect ratio. A greater dimple aspect ratio will reduce the optimum dimple density. The tape/guide minimum spacing does not affect the optimum dimple density.
- The optimum dimple aspect ratio for maximum average air bearing pressure was found to be 0.006, almost independent of the dimensionless tape/guide spacing δ and the flow factor λ.
- The friction coefficient decreases monotonically with increasing dimple aspect ratio. Our simplified model shows good qualitative agreement with experimental results.
- The transition speed between boundary and hydrodynamic lubrication is reduced for a dimpled guide compared to a smooth guide.
- Improvements to the present model can be obtained by including elasto-hydrodynamic effects.

References

1. Richards, D.B., Sharrock, M.P.: Key issues in the design of magnetic tape for linear systems of high track density. IEEE Trans. Magn. **34**(4), 1878–1882 (1998)
2. Taylor, R.J., Talke, F.E.: Investigation of roller interactions with flexible tape medium. Tribol. Int. **38**, 599–605 (2005)
3. Raeymaekers, B., Talke, F.E.: Lateral motion of an axially moving tape on a cylindrical guide surface. J. Appl. Mech. Trans. ASME, doi: 10.1115/1.2723823 (2007)
4. Ono, K.: Lateral motion of an axially moving string on a cylindrical guide surface. J. Appl. Mech. Trans. ASME **46**, 905–912 (1979)
5. Taylor, R.J., Strahle, P., Stahl, J., Talke, F.E.: Measurement of cross-track motion of magnetic tapes. J. Info. Storage Proc. Syst. **2**, 255–261 (2000)
6. Raeymaekers, B., Etsion, I., Talke, F.E.: The influence of design and operating parameters on the magnetic tape/guide friction coefficient. Tribol Lett **25**(2), 161–171 (2007)
7. Raeymaekers, B., Etsion, I., Talke, F.E.: Enhancing tribological performance of the magnetic tape/guide interface by laser surface texturing. Tribol. Lett. **27**(1), 89–95 (2007)
8. Scott, D.A., Brandt, M., Dorien-Brown, B., Valentine, B., De, P.: Laser modification of metal surfaces. Opt. Laser Eng. **18**, 1–13 (1993)
9. Duffet, G., Sallamand, P., Vannes, A.B.: Improvement in friction by cw Nd:YAG laser surface treatment on cast iron cylindrical bore. Appl. Surf. Sci. **205**, 289–296 (2003)
10. Erdemir, A.: Review of engineered tribological interfaces for improved boundary lubrication. Tribol. Int. **38**, 249–256 (2005)
11. Etsion, I.: State of the art in laser surface texturing. J. Tribol. Trans. ASME **27**, 248–253 (2005)
12. Hashimoto, H., Okajima, M.: Theoretical and experimental investigations into spacing characteristics between roller and three types of webs with different permeabilities. J. Tribol. Trans. ASME **128**, 267–274 (2006)
13. Lacey, C., Talke, F.E.: A tightly coupled numerical foil bearing solution. IEEE Trans. Magn. **26**(6), 3039–3043 (1990)
14. Patir, N., Cheng, H.S.: Average flow model for determining effects of 3-dimensional roughness on partial hydrodynamic lubrication. J. Lubr. Technol. Trans. ASME **100**(1), 12–17 (1978)
15. Kligerman, Y., Etsion, I.: Analysis of the hydrodynamic effects in a surface textured circumferential gas seal. Tribol. Trans. **44**(3), 472–478 (2001)
16. Feldman, Y., Kligerman, Y., Etsion, I.: A hydrostatic laser surface textured gas seal. Tribol. Lett. **22**(1), 21–28 (2006)
17. Hirsch, C.: Numerical Computation of Internal and External Flows, vol. 1. John Wiley and Sons, New York (1988)
18. McCool, J.I.: Relating profile instrument measurements to the functional performance of rough surfaces. J. Tribol. Trans. ASME **109**, 264–270 (1987)
19. Eshel, A., Elrod, H.G.: The theory of the infinitely wide, perfectly flexible, self-acting foil bearing. J. Basic Eng. Trans. ASME **87**, 831–836 (1965)
20. Hempstock, M.S., Sullivan, J.L.: The durability and signal performance of metal evaporated and metal particle tape. IEEE Trans. Magn. **32**(5), 3723–3725 (1996)
21. Hempstock, M.S., Sullivan, J.L.: A study of the mechanical and magnetic performance of metal evaporated tape. J. Magn. Magn. Mater. **155**, 323–328 (1996)